# Engineering SERS via absorption control in novel hybrid Ni/Au nanovoids

**Robin M. Cole,[1] Sumeet Mahajan,[1*] Phil N. Bartlett,[2] and Jeremy J. Baumberg,[1]**

[1] *NanoPhotonics Centre, Cavendish Laboratory, University of Cambridge, Cambridge, UK*

[2] *School of Chemistry, University of Southampton, Southampton, UK*

[*] *sm735@cam.ac.uk*

**Abstract:** Nanoscale voids (or '*anti-nanoparticles*') embedded in gold films possess plasmon modes with a strong field component at the cavity entrance, radically different to nanoparticle plasmon modes. By creating Ni/Au hybrid rim nanostructures we show how selective coupling to void plasmons provides strong electric field enhancements leading to large surface-enhanced Raman scattering (SERS) signals from molecules adsorbed on the nanovoid film. Since the rim plasmon modes are relatively independent of the supporting void material these results pave the way for hybrid nanovoid structures which combine plasmonic and catalytic properties of the constituent materials in a controllable and reproducible way.



**OCIS codes:** (190.0190) Nonlinear optics; (220.0220) Optical design and fabrication.

## References and links

1. A. Otto, "Excitation of nonradiative surface plasma waves in silver by the method of frustrated total reflection " Z. Phys. **216**, 398-410 (1968).
2. R. H. Ritchie, E. T. Arakawa, J. J. Cowan, and R. N. Hamm, "Surface-plasmon resonance effect in grating diffraction," Phys. Rev. Lett. **21**, 1530 (1968).
3. T. A. Kelf, Y. Sugawara, R. M. Cole, J. J. Baumberg, M. E. Abdelsalam, S. Cintra, S. Mahajan, A. E. Russell, and P. N. Bartlett, "Localized and delocalized plasmons in metallic nanovoids," Phys. Rev. B **74** (2006).
4. L. Cui, S. Mahajan, R. M. Cole, B. Soares, P. N. Bartlett, J. J. Baumberg, I. P. Hayward, B. Ren, A. E. Russell, and Z.-Q. Tian, "UV SERS at well ordered Pd sphere segment void (SSV) nanostuctures " Phys. Chem. Chem. Phys. **11**, 1023-1026 (2008).
5. S. Mahajan, M. Abdelsalam, Y. Suguwara, S. Cintra, A. Russell, J. Baumberg, and P. Bartlett, "Tuning plasmons on nano-structured substrates for NIR-SERS," Phys. Chem. Chem. Phys. **9**, 104-109 (2007).
6. D. Matthias, and N. Lukas, "Optical frequency mixing at coupled gold nanoparticles," Phys. Rev. Lett. **98**, 026104 (2007).
7. A. L. Demming, F. Festy, and D. Richards, "Plasmon resonances on metal tips: Understanding tip-enhanced Raman scattering," J. Chem. Phys. **122**, 184716 (2005).
8. R. M. Stockle, Y. D. Suh, V. Deckert, and R. Zenobi, "Nanoscale chemical analysis by tip-enhanced Raman spectroscopy," Chem. Phys. Lett. **318**, 131-136 (2000).
9. R. M. Cole, J. J. Baumberg, F. J. Garcia de Abajo, S. Mahajan, M. Abdelsalam, and P. N. Bartlett, "Understanding plasmons in nanoscale voids," Nano Lett. **7**, 2094-2100 (2007).
10. S. Mahajan, R. M. Cole, B. Soares, S. Pelfrey, A. Russell, J. Baumberg, and P. N. Bartlett, "Relating SERS intensity to specific plasmon modes on sphere segment void surfaces," J. Phys. Chem. C **113**, 9284-9289 (2009).
11. Z.-Q. Tian, B. Ren, and D.-Y. Wu, "Surface-enhanced Raman scattering:From noble to transition metals and from rough surfaces to ordered nanostructures," J. Phys. Chem. B **106**, 9463-9483 (2002).
12. B. Ren, Q. J. Huang, W. B. Cai, B. W. Mao, F. M. Liu, and Z. Q. Tian, "Surface Raman spectra of pyridine and hydrogen on bare platinum and nickel electrodes," J. Electroanal. Chem. **415**, 175-178 (1996).
13. Z. Q. Tian, and B. Ren, "Adsorption and reaction at electrochemical interfaces as probed by surface-enhanced Raman spectroscopy," Ann. Rev. Phys. Chem. **55**, 197-229 (2004).

#112987 - $15.00 USD Received 17 Jun 2009; revised 8 Jul 2009; accepted 9 Jul 2009; published 20 Jul 2009

14. Z.-Q. Tian, B. Ren, J.-F. Li, and Z.-L. Yang, "Expanding generality of surface-enhanced Raman spectroscopy with borrowing SERS activity strategy," Chem.l Commun. 3514-3534 (2007).
15. S. Park, P. Yang, P. Corredor, and M. J. Weaver, "Transition metal-coated nanoparticle films: Vibrational characterization with Surface-enhanced Raman scattering," J. Am. Chem. Soc. **124**, 2428-2429 (2002).
16. P. N. Bartlett, J. J. Baumberg, P. R. Birkin, M. A. Ghanem, and M. C. Netti, "Highly ordered macroporous gold and platinum films formed by electrochemical deposition through templates assembled from submicron diameter monodisperse polystyrene spheres," Chem. Mater. **14**, 2199-2208 (2002).
17. P. N. Bartlett, P. R. Birkin, and M. A. Ghanem, "Electrochemical deposition of macroporous platinum, palladium and cobalt films using polystyrene latex sphere templates," Chem. Commun.. 1671-1672 (2000).
18. P. N. Bartlett, P. R. Birkin, M. A. Ghanem, and C.-S. Toh, "Electrochemical syntheses of highly ordered macroporous conducting polymers grown around self-assembled colloidal templates," J. Mater. Chem. **11**, 849-853 (2001).
19. P. N. Bartlett, T. Dunford, and M. A. Ghanem, "Templated electrochemical deposition of nanostructured macroporous PbO2," J. Mater. Chem. **12**, 3130-3135 (2002).
20. P. N. Bartlett, M. A. Ghanem, I. S. El Hallag, P. de Groot, and A. Zhukov, "Electrochemical deposition of macroporous magnetic networks using colloidal templates," J. Mater. Chem. **13**, 2596-2602 (2003).
21. P. N. Bartlett, J. J. Baumberg, S. Coyle, and M. E. Abdelsalam, "Optical properties of nanostructured metal films," Faraday Discuss. **125**, 117-132 (2004).
22. N. D. Denkov, O. D. Velev, P. A. Kralchevsky, I. B. Ivanov, H. Yoshimura, and K. Nagayama, "Mechanism of formation of two-dimensional crystals from latex particles on substrates," Langmuir **8**, 3183-3190 (1992).
23. A. S. Dimitrov, and K. Nagayama, "Continuous convective assembling of fine particles into two-dimensional arrays on solid surfaces," Langmuir **12**, 1303-1311 (1996).
24. P. Jiang, J. F. Bertone, K. S. Hwang, and V. L. Colvin, "Single Crystal colloidal multilayers of controlled thickness," Chem. Mater. **11**, 2132-2140 (1999).
25. J. J. Baumberg, T. Kelf, Y. Sugawara, S. Cintra, M. Abdelsalam, P. N. Bartlett, and A. E. Russell, "Angle-resolved surface-enhanced Raman scattering on metallic nanostructured plasmonic crystals," Nano Lett. **5**, 2262-2267 (2005).
26. M. Moskovits, "Surface-enhanced spectroscopy," Rev. Mod. Phys. **57** (1985).
27. M. Moskovits, "Surface-enhanced Raman spectroscopy: A brief retrospective," J. Raman Spectrosc. **36**, 485-496 (2005).
28. N. M. B. Perney, F. J. G. de Abajo, J. J. Baumberg, A. Tang, M. C. Netti, M. D. B. Charlton, and M. E. Zoorob, "Tuning localized plasmon cavities for optimized surface-enhanced Raman scattering," Phys. Rev. B 35426/35421-35425 (2007).
29. E. C. L. Ru, and P. G. Etchegoin, "Rigourous justification of the $E^4$ enhancement factor in surface enhanced Raman spectroscopy," Chem. Phys. Lett. **423**, 63-66 (2006).
30. A. Ulman, "Formation and structure of self-assembled monolayers," Chem. Rev. **96**, 1533-1554 (1996).
31. J. C. Love, L. A. Estroff, J. K. Kriebel, R. G. Nuzzo, and G. M. Whitesides, "Self-assembled monolayers of thiolates on metals as a form of nanotechnology," Chem. Rev. **105**, 1103-1169 (2005).
32. Z. Mekhalif, J. Riga, J. J. Pireaux, and J. Delhalle, "Self-assembled monolayers of n-dodecanethiol on electrochemically modified polycrystalline nickel surfaces," Langmuir **13**, 2285-2290 (1997).
33. Z. Mekhalif, F. Laffineur, N. Couturier, and J. Delhalle, "Elaboration of self-assembled monolayers of n-alkanethiols on nickel polycrystalline substrates: time, concentration, and solvent effects," Langmuir **19**, 637-645 (2003).

## Introduction

There is currently an intense interest in characterizing and engineering electromagnetic fields in metallic nanoscale structures, as such fields are crucial to applications including surface-enhanced Raman spectroscopy (SERS) and novel metamaterials. The interaction of light with a metal surface can be controlled by structuring the surface on, or below, the scale of the optical wavelength. Using appropriate coupling techniques[1, 2], incident light becomes bound to the metal surface through its interaction with resonant electronic charge oscillations, resulting in propagating and localized surface plasmons. Plasmons can be localized at precise locations, for example on tip features or inside cavity resonators, producing significantly enhanced optical fields. These fields are sensitive to the local geometrical and dielectric environment, allowing the selective modification of bulk optical properties by altering the surface properties at particular locations of a structure.

#112987 - $15.00 USD Received 17 Jun 2009; revised 8 Jul 2009; accepted 9 Jul 2009; published 20 Jul 2009

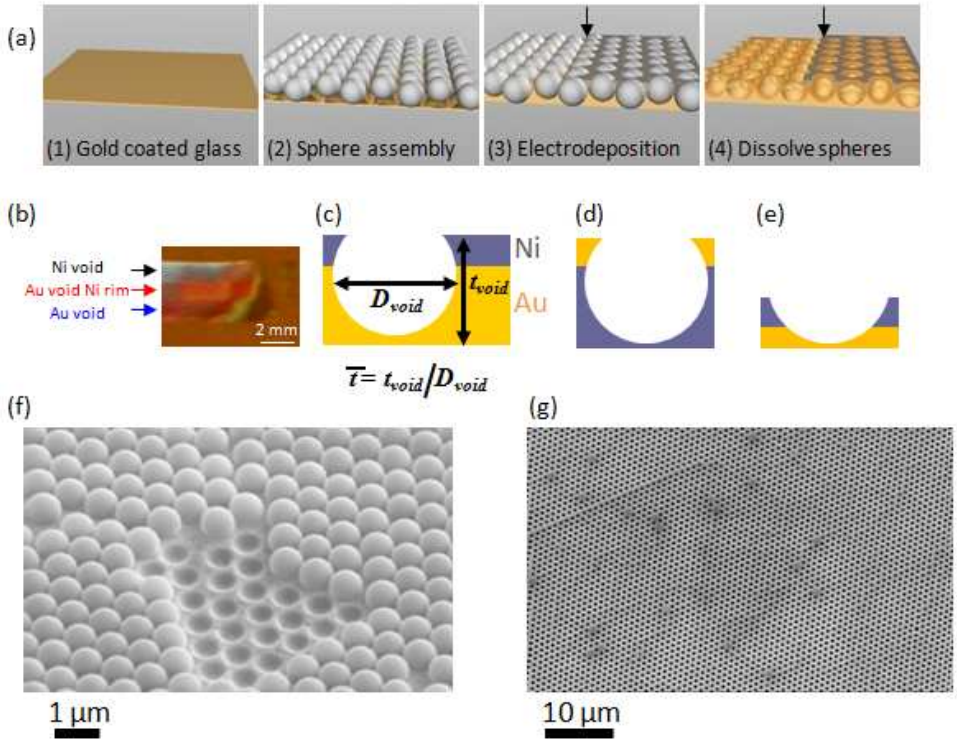


Fig. 1. (a) Sample fabrication procedure utilizing self-assembly of a monolayer of close-packed polymer spheres followed by electroplating. The electroplating is carried out in two steps to create layers of different metals to yield the hybrid nanovoid structure after dissolution of spheres. (b) Microscope image of a nanovoid structure showing regions with nickel voids (black arrow), gold voids with nickel rim (red arrow) and gold voids (blue arrow). (c) Schematic of the nanovoid geometry and definition of normalized thickness $\bar{t}$ . (d) Schematic of hybrid structure designed for novel plasmonic and catalytic properties. (e) Schematic of hybrid 2D photonic crystal designed for long wavelength absorption. SEM images showing (f) a monolayer of spheres embedded in electrodeposited metal and (g) long range order and the large domain size of nanovoid films.

While metallic nanoparticles in close proximity or sharp tips have been the focus of most attention, we have highlighted an alternative nano-*void* plasmon geometry[3], which is much more controllable and reproducible. Such nanovoid structures (Fig. 1, 2) allow rapid investigation of the effects of shape as a function of film thickness ($\bar{t}$) on the observed plasmon modes, as they evolve from open periodic dish structures to fully encapsulated spherical cavities. Reflectivity measurements reveal strong absorption lines in the visible and near-infrared (NIR) spectra, due to the strong coupling of light into surface plasmon modes. We have shown that these plasmon modes can be engineered with great precision, and by tailoring the structure geometry it has been possible to optimize the substrates for SERS in the UV[4] or even in the NIR[5]. Nanovoid surfaces combine the easy coupling of an open spherical geometry embedded in a film with the field-focussing ability of sharp tips in a very controllable and reproducible way, in contrast to studies involving either metallic nanoparticles in close proximity[6] or sharp metal tips brought close to a smooth surface as reported elsewhere[7, 8].

As mentioned earlier the nanovoid geometry supports very different plasmon modes[9] to metal particles or tips. Nanovoids support two distinct types of plasmon mode, which have

#112987 - $15.00 USD Received 17 Jun 2009; revised 8 Jul 2009; accepted 9 Jul 2009; published 20 Jul 2009

energies and coupling strengths which are strongly dependent on the local structure geometry and sample periodicity. For thin films the open periodic dish structures support delocalised Bragg plasmon modes which propagate several microns across a structure, and are so-called due to their coupling by the periodicity of the structure (fully characterized elsewhere[3, 9]). However for thicker films the encapsulated spherical cavities confine and localize plasmons within individual cavities, producing resonances which are referred to as Mie plasmons due to their similarity with the Mie plasmon resonances of particles. The hybrid nanostructures investigated here utilize localised Mie resonances to investigate the influence of thin metal coatings on the plasmonic properties of individual cavities. Furthermore, since Mie resonances are localised within individual cavities, there is no influence on the optical results presented from defects in the crystal lattice.

Spherically-symmetric Mie plasmon modes in the cavity mix with additional rim plasmon modes to produce "bonding" (lower energy) and "antibonding" (higher energy) hybridized states with significant field enhancements at precise spatial locations. Since the fields are concentrated inside the dielectric cavity (as opposed to around the metal of a nanoparticle system), there is reduced damping in the void structure. The plasmonic electric field enhancement depends on the contribution of both re-radiation (optical loss) and damping (absorption loss), and in these nanovoids is found to result in longer plasmon confinement times (giving narrower plasmon linewidths than for nanoparticle plasmons) and therefore stronger excitation of molecules for SERS. The wide variety and wavelength tunability of the plasmon modes of nanovoids, their reproducibility and repeatability makes these substrates ideal for studying SERS enhancement[10]. Each type of plasmon mode has a unique field distribution within the structure, allowing the investigation of SERS from molecules at specific locations within a single geometry. Calculations have confirmed that plasmon modes with a strong field component at the cavity entrance or rim provide extremely high electric field enhancements, and are dramatically modified by even a small change in the local dielectric environment, for example by coating with another material. Whilst gold is the metal of choice for many plasmonic applications (due to its strong plasmonic properties and ease of fabrication), other transition metals including nickel are avoided for plasmonic applications such as SERS[11]. D-band transitions make nickel highly absorbing in the visible wavelength range and hence it supports only heavily-damped surface plasmons, resulting in extremely weak SERS enhancements[12, 13]. However by fabricating gold-nickel *hybrid* structures it is possible to identify the role of precise geometrical features in defining the plasmonic properties of a nanostructure, and create structures with entirely new plasmonic and SERS properties '*invested*' by the hybrid composite. This strategy is distinct from but greatly improves on the '*borrowed* SERS' concept developed on multilayer coated nanoparticles, which possess only small SERS enhancements, or give substrates with irreproducible properties which are susceptible to pinholes since the metal overlayers are only a few monolayers thick[14, 15]. The process we harness makes growth of such hybrid structures straightforward, allowing us to compare gold rims on nickels voids, with nickel rims on gold voids. These results highlight the complementary roles of enhancement and absorption in SERS.

The well established methodology of electroplating through sub-micron colloidal sphere templates[10, 16-21] is used for fabricating the nanovoid substrates employed in this work. The self assembly and electrodeposition procedures lend themselves ideally to the fabrication of intricate multi-metal hybrid nanoscale structures, as shown in Fig. 1a.

While convective assembly[22, 23] and vertical deposition[24] methods have been used to produce regular 2-D arrays of micro-spheres over large areas, assembly of high quality (less defects, larger crystalline domains) films remains a challenge. We have developed a confined convective assembly method capable of self-assembling monolayers of spheres over areas greater than $1cm^2$. Using this technique, sphere sizes between 350nm and 2μm can be assembled in large single domain areas (Fig. 1g) with few defects. Although such self-

#112987 - $15.00 USD Received 17 Jun 2009; revised 8 Jul 2009; accepted 9 Jul 2009; published 20 Jul 2009

assembly techniques inherently produce packing defects, this technique produces templates with a high degree of order, with single crystalline domains of areas typically greater than 100x100 microns$^2$. Moreover, since the plasmonic effects investigated here are primarily due to the localised resonances of individual cavities, the influence of long range crystal defects is not significant. After template formation the sample is placed in an electrochemical plating bath of the metal constituting the first nanostructure layer. By monitoring the current passing through the bath, the thickness of metal deposited on the surface can be accurately controlled. The plated metal fills the interstitial regions between the micro-spheres with growth proceeding from the gold coated glass slide upwards through the spheres. Gold has been deposited using ECF60 (Metalor) electroplating bath containing E3 brightener (Metalor). Nickel has been electroplated using a home-made Watt's bath with p-TSA (para-toluene sulfonic acid) added to it. The conditions have been chosen to given low surface roughness by addition of brightener and surfactant, respectively. By systematically retracting the sample from the plating solution during growth, a sample of graded thickness $\bar{t}$ (defined in Fig. 1c) is produced on a single substrate. For electrodeposition above $\bar{t}$ >0.5, film growth is slower near the edges in contact with the hydrophobic polystyrene spheres, possibly due to diffusion constraints. This results in 'billowing' of the metal film between the spheres (Fig. 3k, l), which is not represented in the model structures (Fig. 3i). Another observed feature of the templated electrodeposition process is that the 'rim' of the structures is not sharp and typically has a roundness of around 50 nm or greater. After plating the first metal, one half of the graded substrate is coated with an insulating paint to isolate it from further electrochemical coating. The sample is then placed in a second plating bath and a uniform thickness of a different metal is deposited around the sphere template and over the first layer. Since the polymer spheres remain embedded in the structure, the second metal layer gets plated on the exposed top surface of the nanostructure only. After plating, the initial sphere template and the insulating paint are completely removed by dissolution in an organic solvent. Using this procedure, graded gold voids with nickel rim hybrid structures are fabricated. The nickel coating layer can subsequently be chemically etched completely to expose the underlying gold structure. For comparison, the inverse structure of graded nickel voids coated with gold tops was similarly prepared.

A gold nanovoid sample of sphere diameter $D$ = 600 nm and thickness grading, $\bar{t}$ = 0.3 – 0.8, is shown in Fig. 2. Initially the sample is plated with two thicknesses of nickel along different longitudinal sections, a thin (~10 nm) and a thick (~ 75 nm) layer. Optical microscope images (Fig. 2 panels b, f and j) show the contrast in colouration between the thin and thick nickel strips, highlighted at three key sample thicknesses ($\bar{t}$ ). SEM images confirm nickel plating only on the *top* surface of the structure and the *rim* entrance to cavities, with smooth gold clearly visible only *within* the cavities. This allows the optical and SERS properties of rim plasmons to be clearly identified and differentiated from plasmons located *within* voids. After the initial experiments were performed, the nickel was completely stripped off the structure by chemical etching, leaving bare gold nanovoids for comparison.

#112987 - $15.00 USD Received 17 Jun 2009; revised 8 Jul 2009; accepted 9 Jul 2009; published 20 Jul 2009

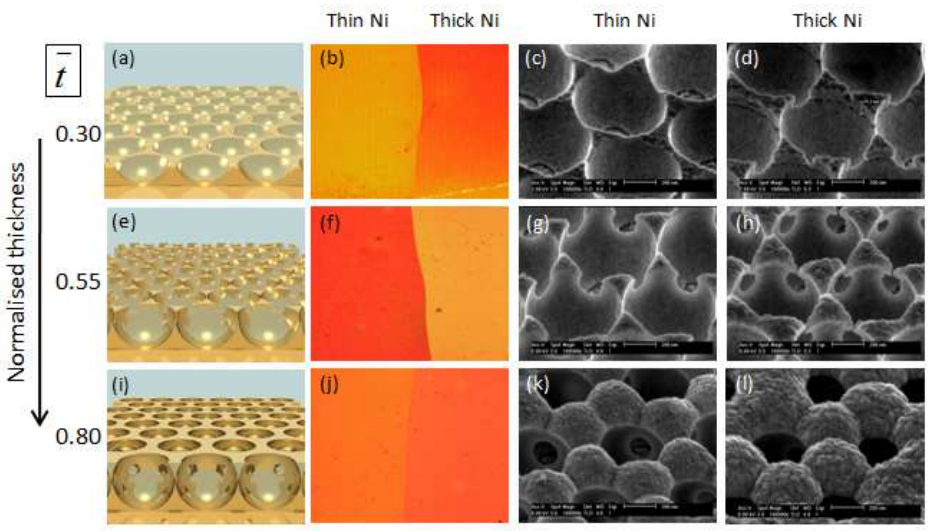


Fig. 2. (a, e, j) Schematic of gold nanovoids at different normalised thickness, $\bar{t}$ . (b, f, j) Microscope images at ×10 show the resulting color change for each nanovoid structure upon nickel coating. SEM images for (c, g, k) thin and (d, h, l) thick nickel coatings on Au structures with the specified $\bar{t}$ .

Whilst images and spectra recorded using an optical microscope reveal clear differences between the gold and nickel-gold hybrid structures, they provide only limited information about the plasmon modes responsible for the dramatic colour contrasts observed. By comparing angle-resolved reflectivity measurements with calculations, it is possible to identify and label the observed plasmon modes. The full dispersion of plasmons was investigated by recording the reflectivity spectrum for different incident angles, $\theta$, and sample azimuthal orientations, $\varphi$, and for various total sample thicknesses $\bar{t}$ , and hence geometries. A super-continuum white-light laser was used to study absorption features throughout the visible and infrared spectral regions with samples mounted on a custom-built computer-controlled goniometer. This is programmed to rotate in both the $\theta$ and $\varphi$ directions as well as move in the *x*-*y* plane of the sample. Spectra are collected using both visible and infrared spectrometers controlled via the same software used to operate the goniometer. The data collected is then combined into a four-dimensional matrix, R($\theta$, $\varphi$, $\bar{t}$ , λ), where it can be viewed and analysed. Angle-resolved reflectivity plots for gold/nickel nanovoid structures of thickness $\bar{t}$ =0.55 and 0.8 are shown as colour plots in Fig. 3, where white corresponds to 100% absorption and blue corresponds to 100% reflection. The first row presents data for $\bar{t}$ =0.55 structures. The gold-only structure (Fig. 3a) supports two distinct plasmon modes; a dispersive plasmon mode at ~ 2.1 eV and a localised mode at ~ 1.5 eV. Structures of thickness $\bar{t}$ = 0.1 - 0.4 and $\bar{t}$ = 0.80 - 1 support surface plasmons propagating on the extended flat metal surfaces between voids, referred to as 'Bragg' plasmons due to their diffractive coupling. The energy of Bragg plasmons is strongly dependent on their in-plane wave-vector and the orientation of the crystal lattice $\varphi$, as seen for the dispersive mode around 2.1 eV (black dashed line). Comparison with calculation[4] reveals the mode at ~1.4 eV to be the $^1P_+$ localised plasmon (Fig. 3f-j). This hybridized mode is composed of a rim mode mixed with a void mode (Fig. 3m), resulting in a strong electric field located at the rim of the cavity. The antibonding configuration of this mode is referred to as the $^1P_-$ mode and again has a strong field component located at the rim of the structure (Fig. 3n). Crucially for comparison with experiment, initial calculations of *coated* nanovoids indicate that the mode absorption strengths and field profiles are rather insensitive to the sharpness of the cavity rim for

#112987 - $15.00 USD Received 17 Jun 2009; revised 8 Jul 2009; accepted 9 Jul 2009; published 20 Jul 2009

rounding radi < 100 nm. For the gold void coated with a ~10 nm layer of nickel with $\bar{t}$ = 0.3, (Fig. 2c), the nickel covers only a small surface area, thus only weakly modifying the observed plasmon modes. However a structure with a 75 nm nickel layer (SEM in Fig. 2d) strongly modifies the plasmonic modes (Fig. 3c). The nickel refractive index tunes the Bragg plasmon to a higher energy, as well as blue-shifting the energy of the $^1P_+$ mode. A third mode is observed at 1 eV which is associated with windows which form between neighbouring voids. This mode has also been blue-shifted by the nickel coating, and appears just at the lower energy spectral range of the gold void structure. The nickel structure coated with a 75 nm layer of gold exhibits weaker but similar plasmonic features to the gold structure (Fig. 3d), apart from a slight increase in the absorption strength and linewidth of the $^1P_+$ mode. Finally, the nickel-only structure exhibits very different plasmonic features (Fig. 3e) to the gold-only structure. The diffractive Wood's anomaly is blue-shifted compared to the Bragg plasmon observed on the gold structure. The $^1P_+$ mode (at 1.4 eV) increases in absorption strength and has a broader linewidth, indicative of increased damping and re-radiation by the nickel layer. These results verify the location and nature of plasmon modes on the gold top layer and at the cavity rim, and confirm that these modes are only subtly influenced by the supporting void structure. Effectively the void acts as an antenna, helping to couple incident light to plasmon modes at the rim of the structure.

Absorption for structures of thickness $\bar{t}$ =0.8 (second row of Fig. 3) show two localised plasmon modes at ~ 1.4 eV and 1.9 eV, which are the $^1P_+$ and $^1P_-$ modes respectively. The gold-only structure (Fig. 3f) shows enhanced input coupling to the $^1P_-$ mode at small θ (~10 º) through mixing with a weak Bragg plasmon propagating on the corrugated top metal surface (with calculated dispersion shown by the black dashed lines) and enhanced input coupling to the $^1P_+$ mode at larger θ (~ 40°). Upon coating with increasing thickness of nickel (Fig. 3g,h), the absorption strength and linewidth of the $^1P_+$ and $^1P_-$ modes is increased, revealed more clearly in the extracted absorption spectra summed over incident angles from 0 to 50° shown in Fig. 3k,l. Since these plasmon modes are localised at the cavity rim, they are highly sensitive to the precise material composition of the local structure, resulting in increased damping on coating with nickel. For the gold structure with a 75 nm layer of nickel (Fig. 3h) absorption by the $^1P_+$ and $^1P_-$ modes is almost identical in strength as for a purely nickel structure (Fig. 3j). However the modes are significantly broadened for the nickel-only structure due to increased coupling from the rim modes into the neighbouring absorptive nickel void. Finally for the nickel void with a layer of gold (Fig. 3i) the absorption strength of the $^1P_+$ and $^1P_-$ modes is reduced compared to the purely nickel structure, and is similar in strength to the gold structure with a thin layer of nickel coating. This indicates that the absorption properties of the nanovoids strongly correlate to the metal composition of the rim. A hybrid rim plasmon ($^1P_{+/-}$) has field concentrated at the apex of the rim (Fig. 3o). Although mostly adjacent to gold, field also penetrates the nearby nickel, resulting in increased absorption by this mode when compared to the equivalent mode on a gold-only structure. Simulations confirm that this mode also exists on a gold void with a nickel rim but the plasmon field is concentrated at the nickel apex, resulting in further increased absorption and damping.

Experiments have revealed that localised plasmons are responsible for the large SERS signals observed from nanovoid structures[10, 25]. However not all localised plasmons generate SERS signals with equal efficiency. The accepted electromagnetic theory[26, 27] of SERS indicates that signal strength is proportional to energy density at the molecule (SERS $\propto E^2_{in} \times E^2_{out}$). Thus experimentally recorded SERS signals are a convolution of the time-averaged electromagnetic enhancement factor with the efficiency of coupling into and out of a plasmon mode, and are therefore sensitive to both the radiative and absorptive properties of the mode. By coating the nanovoid structure with an absorptive metal such as nickel at

#112987 - $15.00 USD Received 17 Jun 2009; revised 8 Jul 2009; accepted 9 Jul 2009; published 20 Jul 2009

specific geometrical locations it is possible to identify experimentally the correlation between plasmon field distribution, coupling strength and SERS enhancement on a single sample.

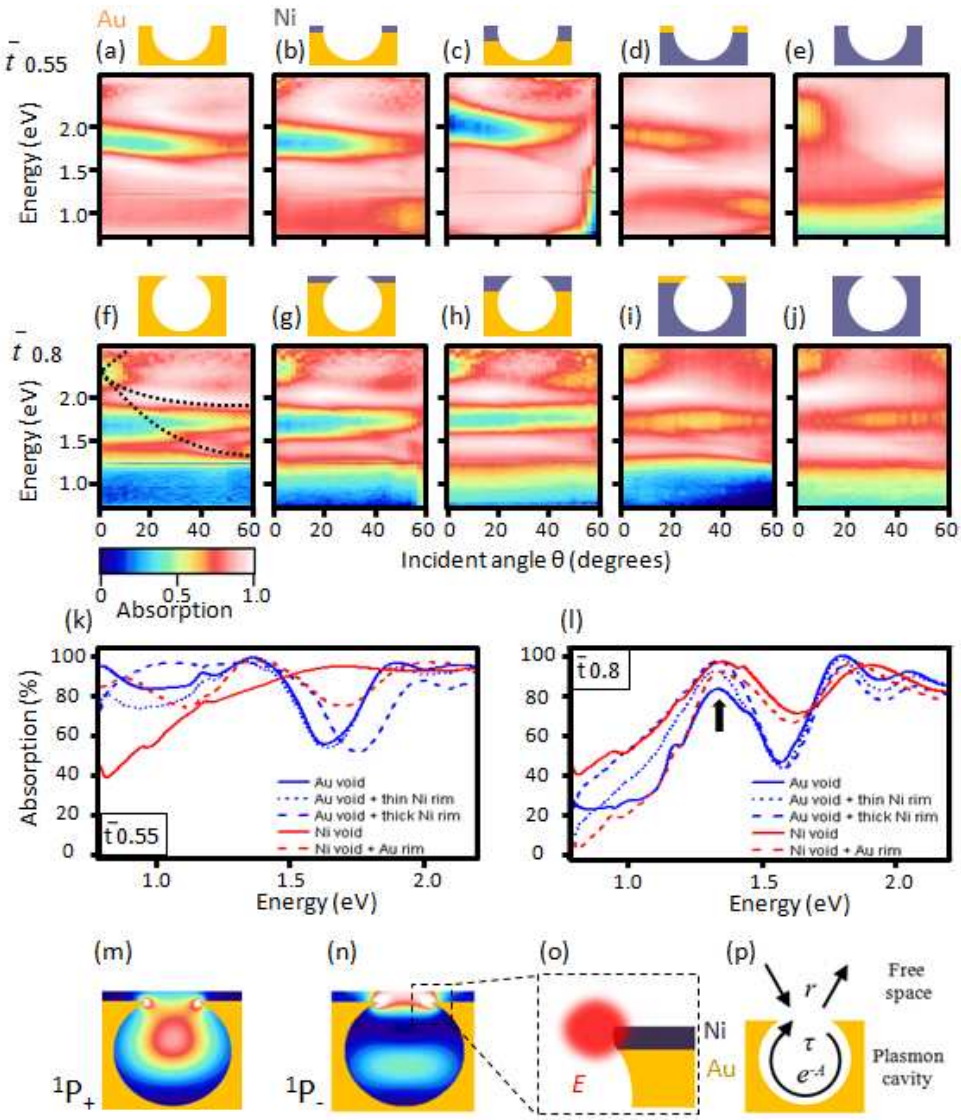


Fig. 3. (a-j) Angle-resolved reflectivity plots for a series of $D$ = 600 nm nanovoid structures of different material compositions. Plots are of normalised reflectivity where blue corresponds to 100% reflectivity and white corresponds to 0% reflectivity. (k, l) Extracted absorption summed over 0 to 50° degrees for comparison with SERS experiments carried out with NA=0.85 objective. (Black arrow indicates energy of extracted absorption peaks shown in Fig. 4c). (m, n) Electric field distribution of the (m) $^1P_+$ and (n) $^1P_-$ localised plasmon modes which have (o) a strong rim component. (p) Schematic of the resonant plasmon cavity model.

SERS measurements are performed on the composite nanovoid structures with benzenethiol used as the probe molecule. Molecules were adsorbed onto the structure by immersion in a 10 mM ethanolic solution for at least 1 h and then thoroughly washed with ethanol. Figure 4a shows the absorption map for a gold nanovoid structure with SERS peak intensities overlaid in blue. Equivalent maps for all structures (not shown) show similar plasmon mode evolution and SERS intensity dependence with thickness, $\bar{t}$, but with the absorption strengths and

#112987 - $15.00 USD Received 17 Jun 2009; revised 8 Jul 2009; accepted 9 Jul 2009; published 20 Jul 2009

linewidths as presented in Fig. 3k,l. The absorption map represents the spectral absorption (summed over incident angles from 0 to 50° which are those collected by the ×100 microscope objective used for SERS measurements) taken at uniformly spaced intervals along the graded nanovoid sample, and is a linear colour plot where yellow corresponds to 100% absorption and black corresponds to 100% reflection. SERS was performed with 785 nm and 633 nm lasers for a single extended scan (10 s integration time) for all samples; dashed lines in Fig. 4a indicate the incident laser wavelength and solid lines are at the absolute wavelength for the 1571 $cm^{-1}$ Raman lines red-shifted from the laser. The marker size on the plot is proportional to the intensity of the SERS peak at each position and is normalized to the maximum SERS intensity obtained with each laser. SERS signals are strongly dependent on the normalized thickness, $\bar{t}$ , with the maximum enhancement observed whenever the incident laser is in resonance with a localised plasmon mode.

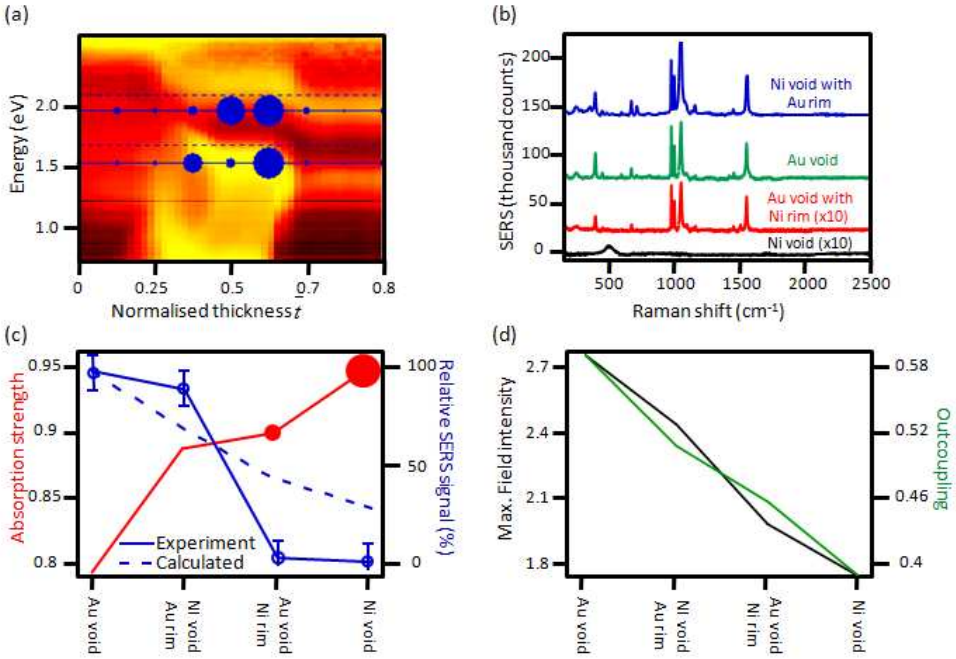


Fig. 4. (a) Absorption map for *D*=600nm gold nanovoid structure graded in thickness $\bar{t}$ , with SERS intensity overlaid in blue, with marker size as the magnitude of the 1571 $cm^{-1}$ line (see text). (b) SERS spectra for 785 nm laser excitation on gold, gold void/nickel rim and nickel void/gold rim structures of thickness $\bar{t}$ = 0.6. The gold void with thicker nickel rim and the nickel-only structures show no observable SERS signals. (c) Measured absorption strength (red) of plasmon modes at $\bar{t}$ = 0.8 with marker size corresponding to FWHM spectral linewidth, compared to observed SERS signal at 785 nm (blue solid line) plotted against rim metal composition ranging from fully gold to fully nickel. The error in SERS signal has been estimated from repeated runs across the sample. Calculated SERS signal from resonant plasmon cavity model (see text) shown dashed. (d) Maximum field intensity and cavity out-coupling calculated using resonant plasmon cavity model.

The absorption map reveals several distinct modes, which tune rapidly in energy with increasing thickness. Comparison with the angle-resolved reflectivity plots of Fig. 3 show that the maximum SERS enhancement is provided by the $^1P_+$ and $^1P_-$ modes which are in resonance with the incident lasers for structures of thickness $\bar{t}$ from 0.4 to 0.8. The gold-only structure and the nickel void with a gold rim give strong SERS signals, however the nickel-only and gold void with nickel rim give negligible SERS signals (Fig. 4b). Although the nickel layer blue-shifts the plasmon resonances slightly with respect to the incident laser, previous

#112987 - $15.00 USD Received 17 Jun 2009; revised 8 Jul 2009; accepted 9 Jul 2009; published 20 Jul 2009

experiments[10] have shown SERS signals to be relatively insensitive to small changes in the resonance energy of the spectrally broad $^1P_+$ and $^1P_-$ modes. Therefore the major factor determining the reduction in SERS strength is the interplay between absorption and radiation provided by the nickel-coated rims.

In order to further elucidate the relationship between light coupling, absorption and SERS signals a simple *resonant plasmon model*[28] is discussed. This model assumes that light couples to plasmons propagating around the length of the cavity *L*, where the field coupling strength of incoming light into the plasmon cavity is $\tau$, with $r$ directly reflected and $r^2 = 1-\tau^2$ The cavity round-trip absorption is $a$, where $a = e^{-A}$ and $A$ is the absorption strength, so that the field surviving a single pass of the cavity $b$ is given by $b^2 = 1-a^2$. Plasmon interference implies that only certain plasmon energies fit within the cavity, leading to a round trip phase $\varphi(\lambda) = Lk_{eff} = L2\pi n_{eff}/\lambda$. Evaluating the multiply-reflected plasmon field, gives the total absorption spectrum

$$\alpha = \frac{\left(1-b^2\right)\left(1-r^2\right)}{\left|1-rbe^{i\phi}\right|^2} \tag{1}$$

Extracting the absorption linewidth in radians ($\Gamma$ is the half-width at half maximum) and the maximum absorption ($\alpha_m$) from equation (1) and inverting the resulting equations gives expressions for the cavity parameters in terms of the measured absorption spectra

$$b^2 = \exp\{-\gamma+\beta\} \tag{2}$$

$$r^2 = \exp\{-\gamma-\beta\} \tag{3}$$

where $\cosh\gamma = 2-\cos\Gamma$ and $\cosh\beta = \alpha_m + (1-\alpha_m)\cosh\gamma$. Hence by measuring $\alpha_m$ and $\Gamma$, we find $b$ and $r$ and hence evaluate the enhanced field intensity, $|E|^2(\lambda) = \left|\varepsilon_{cavity}(\lambda)/\varepsilon_{incident}\right|^2 = \alpha(\lambda)/\left(1-b^2\right)$. It is well known[26, 29] that the SERS intensity for a molecule at $r_i$ is proportional to $\left|E(r_i,\lambda_{in})\right|^2\left|E(r_i,\lambda_{out})\right|^2$. However crucially important in the present hybrid plasmon structures is an additional factor not normally considered. This is the probability, $f_{out}$, that the Raman-shifted plasmon emitted by the molecule will escape as a photon and not be re-absorbed in the metal, where

$$f_{out}^{-1} = 1-\frac{1-b^{-2}}{1-r^2} \tag{4}$$

Calculating the total SERS signals,

$$SERS \propto \left|E_{in}\right|^2\left|E_{out}\right|^2 f_{out} \tag{5}$$

using the extracted values for $\alpha_m$ and $\Gamma$, gives the dashed curve in Fig. 4c, which shows good qualitative agreement with the experimental SERS signals. The SERS signal contributions are broken down into enhanced field intensity $|E|^2$ and out-coupling $f_{out}$ components in Fig. 4d. Because this simple theory assumes the cavity fields to be uniformly distributed, it underestimates the full experimental SERS enhancements which arise from highly localised fields seen in the full cavity field distributions (Fig.3m,n). The simple model however clarifies the relative impact of absorption and re-emission and thus how hybrid structures modify SERS. As the proportion of nickel in the rim is increased, absorption increases and both field intensity and SERS out-coupling are reduced.

#112987 - $15.00 USD Received 17 Jun 2009; revised 8 Jul 2009; accepted 9 Jul 2009; published 20 Jul 2009

Despite this general agreement, the model predicts that the gold void with nickel rim should still give significant SERS signals of about 30% of the signal strength relative to a gold-only structure, whereas in experiments SERS is negligible for this structure. This discrepancy could partly be due to the reduced coverage of SERS probe molecules on nickel compared to gold. While it is firmly established that thiols form well-defined compact monolayers on gold surfaces[30, 31], their attachment to nickel is less efficient due to the presence of NiO on the surface[32, 33]. Hence, some difference in relative coverage between gold and nickel cannot be ruled out. Since the field distribution of the rim plasmon mode (shown in Fig. 3o) is concentrated at the tip apex, SERS signals are critically dependent on the precise location of molecules, magnifying the influence of molecular coverage differences. This implies that the majority of the SERS signal originates from molecules which occupy less than 5% of the available structure surface area from around the rim. Improved hybrid plasmon nanovoid performance for SERS is thus predicted by optimising the thickness of gold on the rim in concert with the supporting nickel void structure to actively concentrate field on molecules located at the gold tip apex.

These experiments confirm that the large SERS signals observed on gold nanovoid structures are provided by rim plasmon modes unique to the nanovoid geometry which are both strongly coupled to incident light by the underlying cavity void (and therefore highly radiative) and provide strong field enhancements localized at the tip apex. Furthermore rim plasmon modes (and corresponding SERS signals) are relatively independent of (and can even be enhanced by) the supporting cavity structure. While here we demonstrate the use of nickel voids with gold rims, it is straightforward to fabricate hybrid nanovoid structures with improved plasmonic and *intrinsic* catalytic properties. Using this geometry, one can envisage monitoring reactions where the reactants are catalysed by the void and the products are monitored at the rim as they emerge out of the nanovoid 'cauldron'. Thus these structures can be employed to study nickel- (or any other transition metal) catalyzed cleavage reactions in solution where the products are SERS active (for which experiments are ongoing). While this opens the possibility of studying products of catalysis in real-time without being forced to use high-vacuum methods from surface science, further tuning of hybrid plasmons will potentially allow reduced separation between SERS-active and catalytically-active regions, which would be of even greater utility as a surface probe.

In summary, gold nanoscale voids have been shown to possess radically different plasmon modes to nanoparticles, with significant field enhancements at the cavity rim responsible for the large SERS signals observed from molecules attached to these structures. By selectively coating the nanovoid structure with a thin layer of nickel the coupling strength, energy and linewidths of the plasmon modes are modified, selectively quenching SERS. Conversely, whilst a nickel void structure supports strong plasmons but does not give SERS, a hybrid structure composed of a nickel void and a gold rim is shown to give SERS signals of similar magnitude to that of a gold only structure. Such experiments identify the precise geometrical location of plasmon modes responsible for SERS, and reveal the subtle relationship between absorption, field coupling and SERS signals using a simple plasmon resonant cavity model. This information is crucial for the effective use of plasmons in antenna applications such as reproducible surface enhanced Raman scattering and paves the way for hybrid structures combining novel plasmonic and catalytic properties simultaneously.

This work was supported by EPSRC grants EP/C511786/1, EP/F059396/1 and EP/G060649/1.

#112987 - $15.00 USD Received 17 Jun 2009; revised 8 Jul 2009; accepted 9 Jul 2009; published 20 Jul 2009